3-D Soft Metamaterials with Negative Poisson's Ratio

Sahab Babaee [*1], Jongmin Shim [†1], James C. Weaver [‡], Elizabeth R. Chen [*], Nikita Patel [*], and Katia Bertoldi [*§]

[*]School of Engineering and Applied Science, Harvard University, Cambridge, MA 02138,[‡]Wyss Institute for Biologically Inspired Engineering, Harvard University, Cambridge, MA 02138,[§]Kavli Institute, Harvard University, Cambridge, MA 02138, and [†]Department of Civil, Structural and Environmental Engineering, University at Buffalo, Buffalo, NY 14260

1 S.B. and J.S. contributed equally to this work.

When materials are uniaxially compressed, they typically expand in directions orthogonal to the applied load. Here, we exploit buckling to design a new class of three dimensional metamaterials with negative Poisson's ratio that contract in the transverse direction under compressive loading regimes. These proposed metamaterials consist of an array of patterned elastomeric spherical shells, which due to a mechanical instability, undergo a significant isotropic volume reduction when deformed. The large geometric non-linearities introduced in the system by buckling are exploited to achieve negative values of Poisson's ratio and retain this unusual property over a wide range of applied deformation. Here, we identify a library of auxetic building blocks and define procedures to guide their selection and assembly. The auxetic properties of these materials are demonstrated both through experimental and finite element simulation approaches and exhibit excellent qualitative and quantitative agreement. As a result of this unusual behavior, these proposed metamaterials could be useful for the design of protective and energy absorbing materials, efficient membrane filters with variable permeability, and acoustic dampeners.

Metamaterials are rationally designed artificial materials which gain their properties from structure rather than composition. Since it was first shown that microstructures built from non-magnetic conducting sheets may exhibit effective magnetic permeability [1], the metamaterial concept has been quickly extended to photonic [2], acoustic [3] and mechanical [4] systems, leading to the design of a variety of materials with properties not accessible in nature.

The Poisson's ratio defines the ratio between the transverse and axial strain [5]. Materials that are uniaxially compressed typically expand in the directions orthogonal to the applied load. Counterintuitively, materials with a negative Poisson's ratio (auxetic materials) contract in the transverse direction [6,7]. The first example of an artificial auxetic material was reported using forms with re-entrant cells that unfolded when stretched [8]. Since then, several periodic 2-D geometries and mechanisms have been proposed to achieve a negative Poisson's ratio [9]. While auxetic responses have been demonstrated in many crystals [10], very few designs of synthetic 3-D auxetic materials have been proposed [4]. Analytical studies have identified 3-D auxetic systems consisting of networks of beams [11], multipods [12] and rigid units [13] and only very recently a metallic 3-D architecture based on a bow-tie functional element has been fabricated [14]. In all these systems, however, the auxetic behavior is exhibited only in the limit of small strains, and the design of 3-D auxetic systems capable of retaining these unusual properties at large strains still remains a challenge [4].

The design of metamaterials capable of responding reversibly to changes in their environment is of fundamental importance for the development of the next generation of actuators and sensors, tunable optics and smart responsive surfaces [15,16]. Furthermore, a remarkable feature of responsive metamaterials is that any of their properties can be switched or fine-tuned just by applying a stimulus to alter their initial architecture.

In order to successfully design a new class of 3-D auxetic materials capable of retaining this unusual response over a wide range of applied strains, we exploit the large geometric non-linearities introduced in the system by instabilities. Through a combination of desktop-scale experiments and finite element (FE) simulations, we investigated the auxetic responses of these structures, finding excellent qualitative and quantitative agreement. Since the 3-D auxetic behavior is induced by elastic buckling, we have named these new materials "Bucklicrystals". We believe that these Bucklicrystals open new design avenues for the construction of 3-D auxetic materials over a wide range of length scales.

We began by recognizing that a structural unit capable of isotropic volume reduction represents the ideal building block to construct 3-D auxetic metamaterials whose response can be controlled by the application of a stimulus. Such responses have been recently demonstrated for patterned spherical shells [17], where a significant change in volume has been observed as a result of an elastic instability. The hole arrangement on the spherical shell has also been explored, showing that only five patterns comprising of 6, 12, 24, 30 and 60 holes are possible for such building blocks [17]. Note that these five spherical structures can be classified into two symmetry groups: the shells with 6, 12 and 24 holes have octahedral symmetry, while those with 30 and 60 holes have icosahedral symmetry.

Having identified the building blocks, we then defined procedures to guide their assembly. Here, we focused on cubic crystal systems (i.e. simple cubic (*sc*), body-centered cubic (*bcc*), and face-centered cubic (*fcc*)) because of their simplicity and highest symmetry order out of the seven lattice systems. Since it was necessary that both the building blocks and the metamaterial have octahedral symmetry, only spherical shells with 6, 12 and 24 holes were considered in this study (Figs. 1a and S1). Furthermore, for the sake of simplicity and ease of scalability, we constructed each metamaterial from a single type of building block.

Since each building block has a limited number of sites where adjacent building blocks can be attached to each other (see markers in Fig. 1a) and metamaterials with octahedral symmetry can be built only via connecting identical junctions (i.e. junctions identified by the same type of markers in Fig. 1a), only six different Bucklicrystals can be built (Figs. 1b and S2): *bcc* crystals using building blocks with 6, 12 and 24 holes, *sc* crystals using building blocks with 12 and 24 holes, and *fcc* crystal using building blocks with 24 holes. Having identified all possible configurations for the Bucklicrystals, we next investigated their response through a combination of experiments and numerical simulations.

We first fabricated and mechanically tested a Bucklicrystal consisting of a *bcc* array of building blocks with 6 holes. Using addi-

Reserved for Publication Footnotes

tive manufacturing for the fabrication of individual molds for each unit cell, we fabricated the building blocks from a soft silicone-based rubber (Vinyl Polysiloxane with Young's modulus, $E = 784\,KPa$). The geometry of the building block comprises a spherical shell (inner diameter $d_i = 19.8\,mm$ and wall thickness $t = 7.1\,mm$) that is patterned with a regular array of 6 circular voids that are slightly tapered ($22\,mm$ and $13\,mm$ maximum and minimum diameter, respectively) (Figs. 1 and S1). Ninety one identical building blocks were fabricated and subsequently joined to form a *bcc* crystal using the same polymer as an adhesive agent.

The Bucklicrystal was then tested under uniaxial compression and the evolution of the microstructure was monitored taking tomographic images at five different levels of the applied nominal strain (calculated as change of height of the sample divided by the original height), $\epsilon_{22}^{\text{applied}} = -0.03, -0.08, -0.15, -0.20, -0.30$, with a micro-CT X-ray imaging machine (HMXST225, X-Tek). Fig. 2 shows isometric and mid-cross sectional views of the structure in the undeformed ($\epsilon_{22}^{\text{applied}} = 0$ - Fig. 2a) and deformed ($\epsilon_{22}^{\text{applied}} = -0.20$ - Fig. 2b) configurations. Furthermore, a sequence of progressively deformed shapes of the inner-most building block at different levels of strain is shown in Fig. 2c. These snapshots clearly demonstrate that structural transformations induced by instabilities occur when the Bucklicrystal is compressed. All the building blocks are found to shrink significantly in all directions and their initially circular holes on the spherical shell transform into elongated, almost closed ellipses. Moreover, Figs. 2a,b clearly show that all of the lateral boundaries of the deformed Bucklicrystal bend inwards, a clear indication of a 3-D negative Poisson's ratio.

Recognizing that the response of the specimens is necessarily influenced by boundary conditions at both the loaded and the traction-free faces, we focused on the inner-most building block (which can be considered as the representative volume element (RVE) for the corresponding infinitely periodic structure) and quantitatively estimated its deformation using image post-processing. First, each tomographic image was size-calibrated using the known shell thickness ($t = 7.1\,mm$), which was only marginally affected by deformation. We then tracked the centroids of the four voids surrounding the RVE in both the 1-2 and the 2-3 planes (see vertices of the red rectangle in Figs. 2a,b) and used them to calculate centroid-to-centroid distances along the three directions, denoted by Δx_1, Δx_2, and Δx_3. Prior to compression, the value for all of these quantities was $\Delta x_i(0) \simeq 38\,mm$, $i = 1, 2, 3$. Local normal strains were then obtained as $\epsilon_{ii} = \langle \Delta x_i \rangle / \Delta x_i(0)$, where the angular bracket $\langle \cdot \rangle$ denotes ensemble average over all distances under consideration. It is worth noting that the measured local longitudinal strains, denoted by ϵ_{22}, were higher than those applied, denoted by $\epsilon_{22}^{\text{applied}}$. This was expected since the building blocks in close proximity of the two plates used to compress the structure were highly constrained by friction and were unable to fully deform.

In Fig. 3a, we present the dependence of the transverse strains ϵ_{11} and ϵ_{33} on the longitudinal strain ϵ_{22}. The error bars on the experimental points were obtained from the standard deviation of the two values of Δx_i used in each averaging. Remarkably, the data clearly show that upon increasing the compressive strain ϵ_{22}, both transverse strains decrease, indicating that the structure contracts in both lateral directions. To quantify these lateral contractions, the Poisson's ratios were calculated from the engineering strain as $\nu_{ij} = -\epsilon_{ii}/\epsilon_{jj}$. The estimates of ν_{ij} were plotted as a function of ϵ_{22} in Fig. 3b. The evolution of ν_{21} and ν_{23} was characterized by two subsequent regimes: a decreasing regime followed by a plateau. Initially both Poisson's ratios monotonically decrease. They became negative at $\epsilon_{22} \simeq -0.03$, and eventually reached the value $\nu \simeq -0.4$ and plateau at $\epsilon_{22} \simeq -0.20$, demonstrating that the response of the Bucklicrystal was auxetic over a wide range of deformations. Finally we note that, since the specimens are made of an elastomeric material, the process was fully reversible and repeatable. Upon release of the applied vertical displacement, the deformed structures recovered their original configurations.

Next, we performed finite element (FE) simulations of the 6-hole Bucklicrystal. To verify that the auxetic behavior measured in the experiments was not affected by the boundary conditions, we considered the structure to be infinite and investigate the response of a representative volume element (RVE) under uniaxial compression using periodic boundary conditions. All analyses were performed on the cubic RVE comprising a central building block connected to one-eighth of the building block at each junction (the junctions and the RVE are shown in Fig. 1a).

We first investigate the stability of the Bucklicrystal through Bloch wave analysis [18, 19]. The analysis detects a mechanical instability at $\epsilon_{22} = -0.03$, leading to a critical mode where all building blocks undergo the same rotation (Figs. 1c-top and S4). The post-buckling response of the Bucklicrystal was then simulated by introducing a small imperfection in the initial geometry. In Fig. 2d we present a sequence of the progressive collapse of the Bucklicrystal obtained from FE simulations, which is in remarkable qualitative agreement with the experiments for the same geometric and material parameters (Fig. 2c). The snapshots clearly revealed that in this Bucklicrystal, mechanical instabilities act as a functional mode of actuation, inducing the spherical collapse of every building block while keeping the structure periodic. To better characterizing the response of the structure, in Fig. 3 we report the evolution of the lateral strains (ϵ_{11}, ϵ_{33}) and Poisson's ratios (ν_{21}, ν_{23}) as a function of ϵ_{22}, showing an excellent quantitative agreement with experiments. It is worth noting that since after buckling, the initial cubic RVE changes into a rectangular parallelepiped, for large values of longitudinal strain $\epsilon_{33} \neq \epsilon_{11}$ and $\nu_{21} \neq \nu_{23}$. This can be clearly seen in Fig. 2d for $\epsilon_{22}^{\text{applied}} = -0.30$, where all the ligaments in the 1-2 plane are touching, while in the 2-3 plane they are still away from each other.

Given the excellent qualitative and quantitative agreement found between experiments and simulations, we proceeded by focusing primarily on the FE simulation results to further explore the buckling-induced auxetic behavior of all the Bucklicrystals identified in Fig. 1. Each building block is fully characterized by two adimensional parameters: porosity, denoted by ψ, (defined as the ratio of the void volume to the intact spherical shell volume) and thickness over inner radius ratio, denoted by t/r_i [17]. All crystals were constructed using building blocks characterized by the same parameters used for the 6-hole crystal investigated above, $\psi = 0.733$ and $t/r_i = 5/7$.

All analyses were performed on cubic RVEs (Fig. 1b and S2): (*i*) for *bcc* configurations (12- and 24-hole), they were constructed as described for the 6-hole *bcc* case; (*ii*) for the *sc* configurations (12- and 24-hole), a single building block was used as RVEs; (*iii*) for the *fcc* configuration (24-hole), RVEs were built such that they comprise of 6 half-building blocks located in the middle of the cube faces, attaching to 8 one-eighth of the building blocks at the corners. It is worth noting that the use of building blocks characterized by the same parameters ψ and t/r_i results in Bucklicrystals with different initial global porosities, denoted by $\bar{\psi}$ (*i.e.* $\bar{\psi}_{sc} = 0.888$, $\bar{\psi}_{bcc} = 0.854$ and $\bar{\psi}_{fcc} = 0.842$). In all Bucklicrystals, instabilities of short wavelength are found to be critical, leading to spherical collapse of all the building blocks. The values of critical strain obtained from Bloch wave analysis were $\epsilon_{22}^{cr} = -0.030, -0.030, -0.041, -0.020, -0.026$, and -0.023 for 6-hole *bcc*, 12-hole *bcc* and *sc*, and 24-hole *bcc*, *sc* and *fcc*, respectively. Moreover, the deformed mode shape of the RVEs are reported in Fig. 1c. Note that for the *sc* configurations, when the critical instability occurs, the periodicity of the crystal is altered and a new RVE comprises of 8 building blocks is found (RVE size = $2 \times 2 \times 2$ in 1, 2, and 3 directions). Furthermore, differently from the 6-hole Bucklicrystal, where buckling is found to induce the same rotation in all building blocks, in all the other crystals each building block rotates

in the opposite direction with respect to the surrounding connected units.

A more quantitative comparison between the response of all the Bucklicrystals can be made by inspecting the evolution of stresses and Poisson's ratios. Fig. 4 shows the evolution of the normalized nominal stress S_{22}/E as a function of the longitudinal strain ϵ_{22}. The response of all configurations is characterized by a linear elastic regime followed by a stress plateau. The departure from linearity is the result of buckling and corresponds to a sudden transformation in the periodic pattern as shown in Fig. 4c, where snapshots of undeformed and deformed ($\epsilon_{22} = -0.15$) configurations are presented. Note that all the crystals are uniaxially compressed up to the limit when the ligaments surrounding the holes begin to contact one another. This results in a maximum longitudinal strain $\epsilon_{22} \simeq -0.30$ for all the crystals, except the *bcc* crystal comprising of an array of 24 holes building blocks in which the ligaments come into contact with each other at $\epsilon_{22} \simeq -0.15$.

The evolution of the Poisson's ratios as function of ϵ_{22} is also presented in Fig. 4b. All the Bucklicrystals are characterized by initial positive values of ν, a steeply decreasing regime initiated at the onset of instability, and a final negative plateau by further compression. Therefore, in all the Bucklycrystals, an evolution of the Poisson's ratio from positive to negative is observed; this transition occurs first in the 24-hole *fcc* Bucklicrystal (at $\epsilon_{22} \simeq -0.04$) and last in the 12-hole *sc* (at $\epsilon_{22} \simeq -0.12$). Remarkably, once the crystals become auxetic, they retain this unusual properties even at large strains. At $\epsilon_{22} = -0.30$, all configurations are characterized by negative Poisson's ratio, ranging from -0.2 for the 12-hole *bcc* crystal to -0.5 for the 24-hole *fcc*. Finally, we note that all the crystals, except the 6-hole case, retain the transversely symmetric behavior (i.e. $\nu_{21} = \nu_{23}$) even at large strains.

Our finding of buckling-induced auxetic behavior provides a fundamentally new way for generating 3-D materials with a negative Poisson's ratio. Our results offer a unique mechanism with a range of advantages: (*i*) the proposed design rules can be applied to various length-scales; (*ii*) the reconfiguration can occur upon application of different stimuli depending on the types of materials; (*iii*) the transformation can be made fully reversible; and (*iv*) the auxetic behavior is retained over a wide range of applied strain. From a practical perspective, the full control over the desired outcome in combination with the wealth of different length scales, materials, stimuli, and geometrical designs provides reversibly auxetic architectures with a broad field of applications ranging from energy absorbing materials to tunable membrane filters. Finally, although mechanical instabilities have been traditionally viewed as a failure mode with research focusing on how to avoid them, here we change this prospective and exploit instabilities to design a new class of 3-D auxetic materials.

Materials and Methods

Materials. A silicone-based rubber (commercial name: Elite Double 32, Zhermack) was used to cast the experimental specimen. The material properties were measured through tensile testing, up to the true strain of $\epsilon = 0.60$. No hysteresis was found during loading and unloading. The constitute behavior was accurately captured by a Yeoh hyperelastic model [20], whose strain energy is $U = \sum_{i=1}^{3} C_{i0} \left(\bar{I}_1 - 3\right)^i + (J-1)^{2i} / D_i$ where $C_{10} = 131\, KPa$, $C_{20} = 0\, KPa$, $C_{30} = 3.5\, KPa$, $D_1 = D_2 = D_3 = 154\, GPa^{-1}$. Here, $\bar{I}_1 = \mathrm{tr}\left[\mathrm{dev}\left(\mathbf{F}^T\mathbf{F}\right)\right]$, $J = \det\mathbf{F}$, and $\mathbf{F}$ is the deformation gradient. Two of the Yeoh model parameters are related to the conventional shear modulus, denoted by G_0 , and bulk modulus, denoted by K_0 , at zero strain: $C_{10} = G_0/2$, $D_1 = 2/K_0$.

Fabrication of the building blocks. A mold was fabricated using a 3-D printer (Objet Connex500) to cast one half of a spherical shell. After de-molding, two halves were joined using the same polymer as adhesive agent. The specimen fabricated for this study has the thickness of $t = 7.1\, mm$, the inner diameter of $d_i = 19.8\, mm$, and the outer diameter of $d_o = 34.0\, mm$.

Testing of the Bucklicrystal. After preparing 91 spherical shells, all the shells were joined using the same polymer as adhesive agent. The dimension of the Bucklicrystal was $\mathrm{Height} \times \mathrm{Width} \times \mathrm{Depth} = 144.0 \times 141.0 \times 141.0\, mm$. In order to observe the evolution of the Poisson's ratio of the Bucklicrystal, we applied five different levels of vertical deformation, i.e. engineering strains of $\epsilon_{22} = -0.03,\ -0.08,\ -0.15,\ -0.20$ and -0.30 with respect to the height of the Bucklicrystal. At the strain level of interest, we immobilized the specimen using a fixture made of acrylic plates, nylon bolts/nuts and inch-thick closed-cell foam plates placed between the specimen and the fixture (Fig. S3). The foam plates were used as a low electron density spacer that would be nearly invisible in the acquired x-ray transmission images and thus not interfere with volume rendering of the higher electron density silicone elastomer Bucklicrystal. The specimen with the fixture was put into a micro-CT X-ray imaging machine (HMXST225, X-Tek) to take its tomographic images. Once its 3-D images of the inside of the the specimen were reconstructed, the cross-sectional views of interest were extracted.

Numerical Simulations. The simulations were carried out using the commercial Finite Element package Abaqus (SIMULIA, Providence, RI). The Abaqus/Standard solver was employed for all the simulations, *i.e.* for both microscopic and macroscopic instability analyses and post-buckling analysis. Models were built using quadratic solid elements (ABAQUS element type C3D10M with a mesh sweeping seed size of $1\, mm$ and the analyses were performed under uniaxial compression. We used first four eigenvalues from instability analysis as imperfection on non-linear post Buckling analysis. More details on the FE simulations are provided in the *SI Text*.

ACKNOWLEDGMENTS. This work has been supported by Harvard MRSEC through grant DMR-0820484 and by NSF through grants CMMI- 1149456 (CAREER) and by the Wyss Institute through the Seed Grant Program. K.B. acknowledges start-up funds from the Harvard School of Engineering and Applied Sciences and the support of the Kavli Institute and Wyss Institute at Harvard University. This work was performed in part at the Center for Nanoscale Systems (CNS), a member of the National Nanotechnology Infrastructure Network (NNIN), which is supported by the National Science Foundation under NSF award no. ECS-0335765. CNS is part of Harvard University.

1. Pendry J, a.J. Holden, Robbins D, Stewart W (1999) Magnetism from conductors and enhanced nonlinear phenomena. *IEEE Transactions on Microwave Theory and Techniques* 47:2075–2084.
2. Soukoulis CM, Wegener M (2011) Past achievements and future challenges in the development of three-dimensional photonic metamaterials. *Nature Photonics* 5.
3. Lu MH, Feng L, Chen YF (2009) Phononic crystals and acoustic metamaterials. *Materials Today* 12:34–42.
4. Lee JH, Singer JP, Thomas EL (2012) Micro-/nanostructured mechanical metamaterials. *Advanced materials (Deerfield Beach, Fla.)* 24:4782–810.
5. Greaves GN, Greer A, Lakes R, Rouxel T (2011) Poisson's ratio and modern materials. *Nature materials* 10:823–838.
6. Lakes R (1993) Advances in negative Poisson's ratio materials. *Advanced Materials* 5:293–296.
7. Evans KE, Alderson a (2000) Auxetic Materials: Functional Materials and Structures from Lateral Thinking. *Advanced Materials* 12:617–628.
8. Lakes R (1987) Foam Structures with a Negative Poisson's Ratio. *Science (New York, N.Y.)* 235:1038–1040.
9. Liu Y, Hu H (2010) A review on auxetic structures and polymeric materials. *Scientific Research and Essays* 5:1052–1063.
10. Baughman RH, Shacklette JM, Zakhidov AA, Stafstro S (1998) Negative Poisson's ratios as a common feature of cubic metals. *Nature* 392:362–365.
11. Hughes T, Marmier a, Evans K (2010) Auxetic frameworks inspired by cubic crystals. *International Journal of Solids and Structures* 47:1469–1476.
12. Pikhitsa PV, Choi M, Kim HJ, Ahn SH (2009) Auxetic lattice of multipods. *Physica Status Solidi (B)* 246:2098–2101.
13. Attard D, Grima JN (2012) A three-dimensional rotating rigid units network exhibiting negative Poisson's ratios. *Physica Status Solidi (B)* 249:1330–1338.
14. Bückmann T, et al. (2012) Tailored 3D mechanical metamaterials made by dip-in direct-laser-writing optical lithography. *Advanced materials (Deerfield Beach, Fla.)* 24:2710–4.
15. Sidorenko A, Krupenkin T, Taylor A, Fratzl P, Aizenberg J (2007) Reversible Switching of. *Science (New York, N.Y.)* 315:487–490.
16. Bertoldi K, Reis PM, Willshaw S, Mullin T (2010) Negative Poisson's ratio behavior induced by an elastic instability. *Advanced materials (Deerfield Beach, Fla.)* 22:361–6.

17. Shim J, Perdigou C, Chen ER, Bertoldi K, Reis PM (2012) Buckling-induced encapsulation of structured elastic shells under pressure. *Proceedings of the National Academy of Sciences of the United States of America* 109:5978–83.
18. Bertoldi K, Boyce M, Deschanel S, Prange S, Mullin T (2008) Mechanics of deformation-triggered pattern transformations and superelastic behavior in periodic elastomeric structures. *Journal of the Mechanics and Physics of Solids* 56:2642–2668.
19. Geymonat G, Muller S, Triantafyllidis N (1993) Homogenization of Nonlinearly Elastic Materials , Microscopic Bifurcation and Macroscopic Loss of Rank-One Convexity. *Arch. Rational Mech. Anal.* 122:231–290.
20. Yeoh O (1993) Some forms of the strain energy function for rubber. *Rubber Chem. Technol.* 66:754–771.

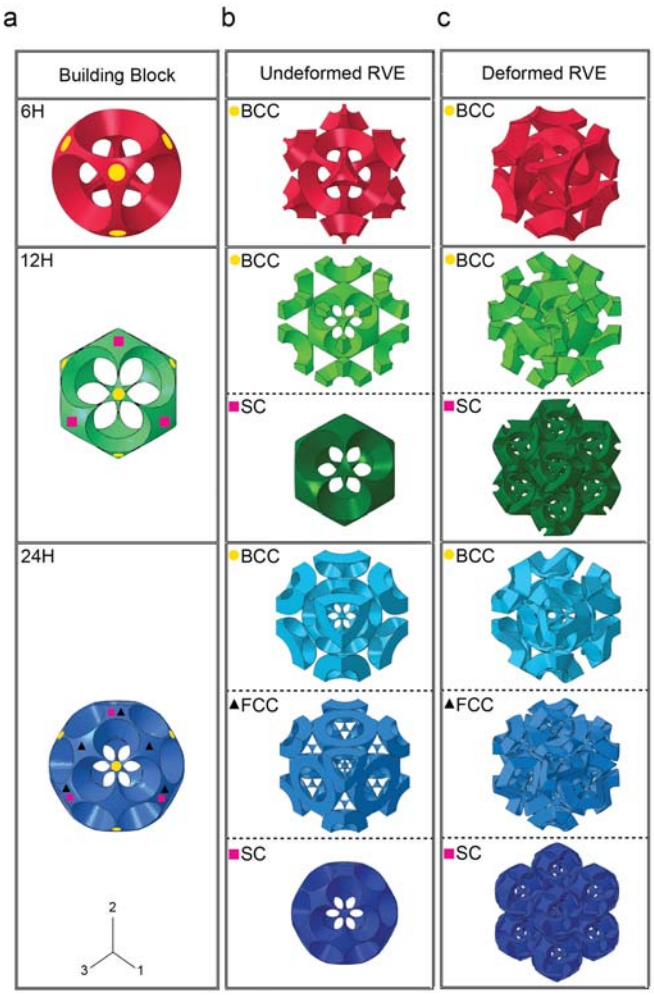

Fig. 1. Gallery of Bucklicrystals. a, Building block with 6, 12 and 24 holes. For the sake of simplicity, we always color the building blocks with 6, 12 and 24 holes with red, green and blue, respectively. Moreover, we also identify the junctions where the building blocks are attached to the surrounding units using yellow circle, black triangle, and magenta square for *bcc*, *fcc*, and *sc* packing configurations, respectively. **b**, Representative volume elements (RVE) for the Bucklicrystal in the undeformed configuration. **c**, Buckled configurations for the RVEs under uniaxial compression.

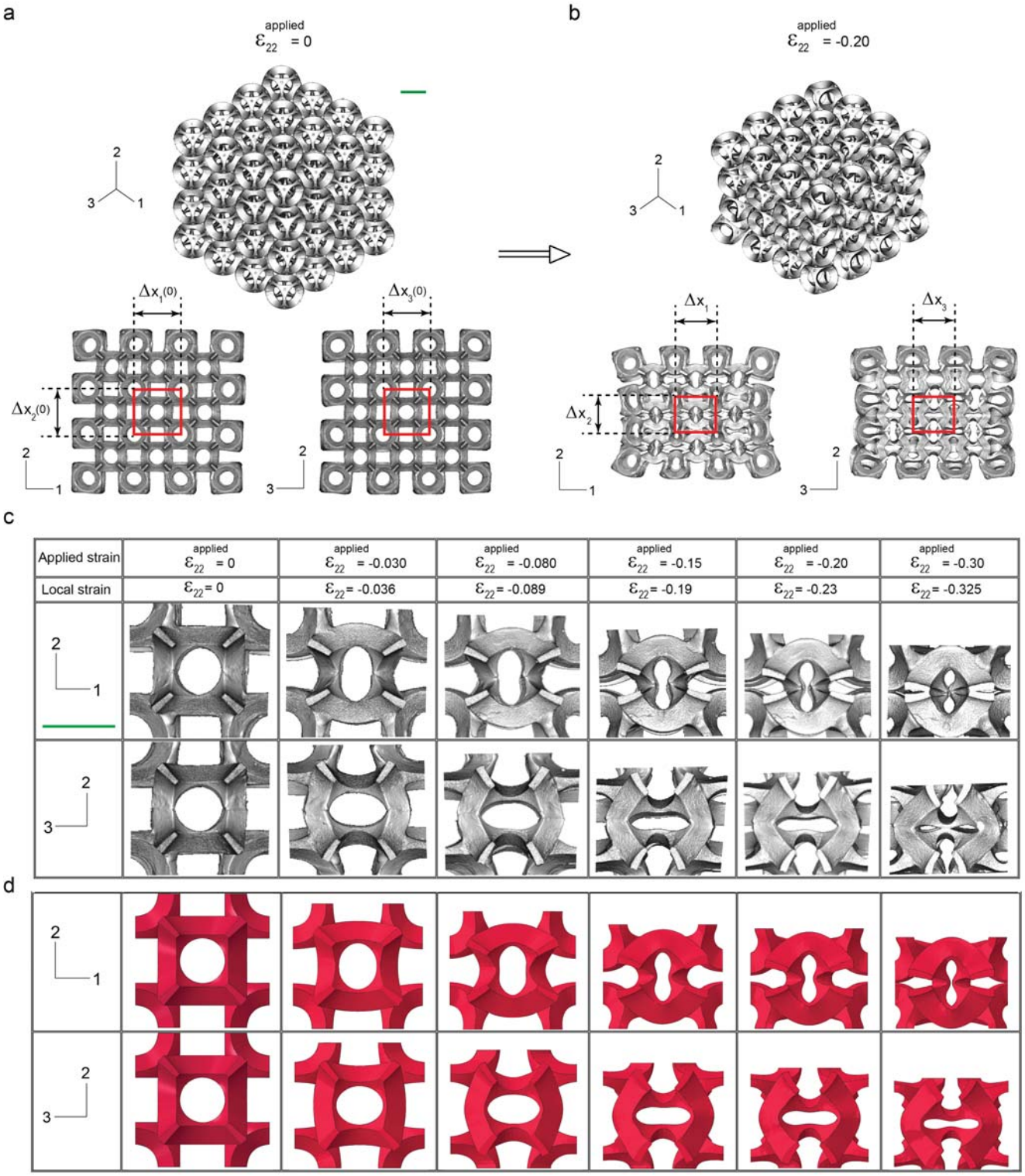

Fig. 2. Experimental (CT X-ray) and numerical images of the 6-hole Bucklicrystal. **a**, Isometric and cross-sectional views of the undeformed crystal from micro-CT X-ray imaging machine. **b**, Isometric and cross-sectional views of the uniaxially compressed crystal ($\epsilon_{22}^{\text{applied}} = -0.20$) from micro-CT X-ray imaging machine. In the cross sectional views the inner-most RVE is highlighted by a red box. $\Delta x_i(0)$ and Δx_i, $i = 1, 2, 3$, are the edge length of the red box in the i direction for undeformed and buckled crystals, respectively. **c**, Magnified views of the inner-most RVE taken from CT X-ray scanning at different levels of strains. **d**, Corresponding pictures taken from simulation. (Green scale bars: $20\,mm$)

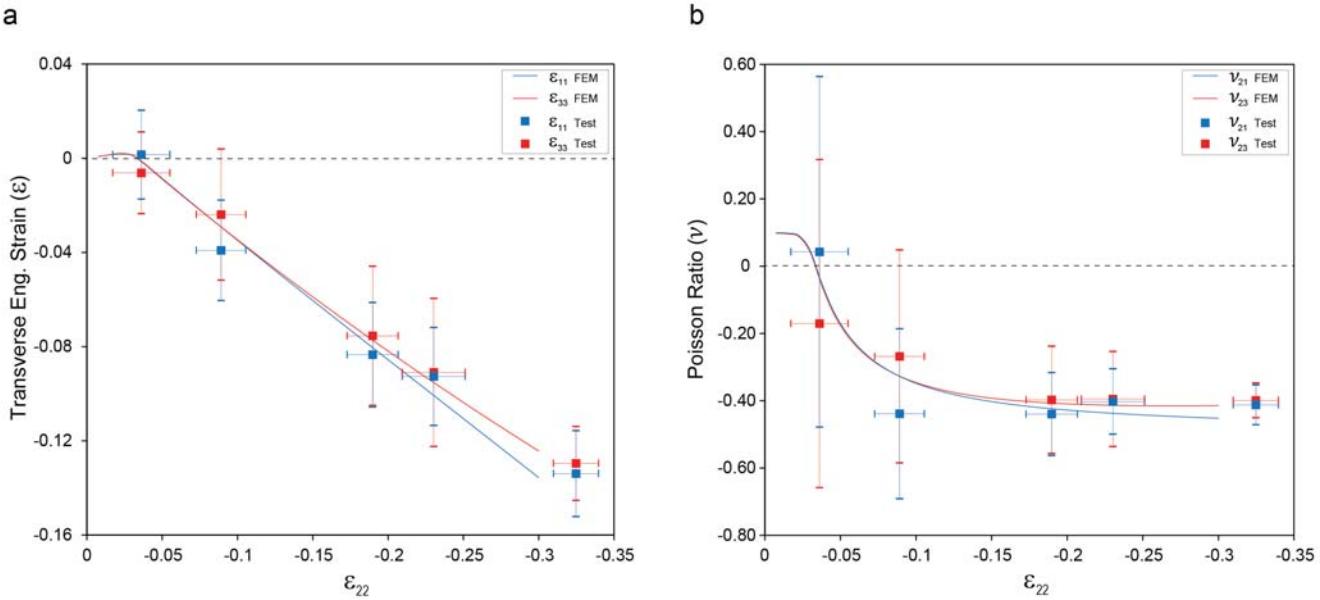

Fig. 3. Evolution of transverse strains and Poisson's ratios for the 6-hole Bucklicrystal. **a**, Evolution of the transverse engineering strain ϵ_{11} and ϵ_{33} as a function of the applied longitudinal strain ϵ_{22}. **b**, Evolution of the Poisson's ratios (ν_{21} and ν_{23}) of the 6-hole Bucklicrystal as a function of compressive strain ϵ_{22}. The finite element results (solid lines) are in good agreement with the experimental data (square markers).

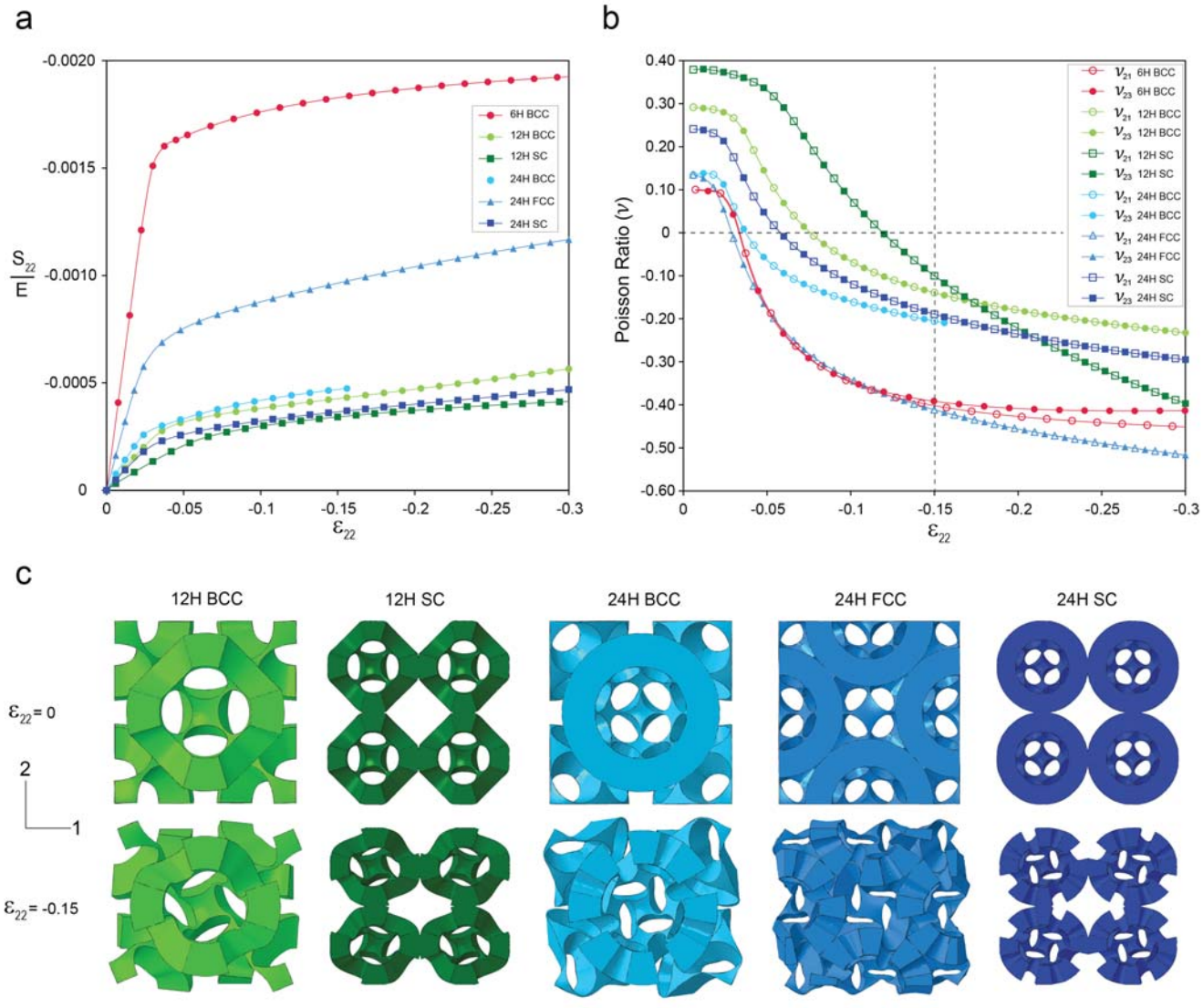

Fig. 4. Mechanical response of Bucklicrystals. **a**, Nominal stress-strain curves from uniaxial compression in 2-direction for all the Bucklicrystals. The stress is normalized with respect to the elastic modulus of the bulk elastomeric material. **b**, Evolution of the Poisson's ratios vs. nominal strain in 2- direction for all the Bucklicrystals. **c**, Cross sectional views of undeformed ($\epsilon_{22} = 0$) and deformed ($\epsilon_{22} = -0.15$) configurations of 12- and 24-hole Bucklicrystals.